Molecular Crystals and Liquid Crystals

Publication details, including instructions for authors and subscription information:
http://www.tandfonline.com/loi/gmcl20

X-RAY STRUCTURAL STUDIES OF FERROELECTRIC LIQUID CRYSTAL DEVICES

Carl Brown [a], Paul E Dunn [a], J Cliff Jones [a], Sam A Jenkins [b] & R M Richardson [b]

[a] DERA, St Andrews Road, Malvern, WR14 3PS, UK

[b] School of Chemistry, Cantocks Close, Bristol, BS8 1TS, UK

Version of record first published: 15 Jul 2010

To cite this article: Carl Brown, Paul E Dunn, J Cliff Jones, Sam A Jenkins & R M Richardson (2003): X-RAY STRUCTURAL STUDIES OF FERROELECTRIC LIQUID CRYSTAL DEVICES, Molecular Crystals and Liquid Crystals, 402:1, 55-75

To link to this article: http://dx.doi.org/10.1080/744816687

Mol. Cryst. Liq. Cryst., Vol. 402, pp. 55/[291]–75/[311], 2003

ISSN: 1542-1406 print/1563-5287 online
DOI: 10.1080/15421400390243336

Taylor & Francis
Taylor & Francis Group

X-RAY STRUCTURAL STUDIES OF FERROELECTRIC LIQUID CRYSTAL DEVICES

Carl Brown[‡], *Paul E Dunn, and J Cliff Jones*[†]
DERA, St Andrews Road, Malvern, WR14 3PS, UK

Sam A Jenkins and R M Richardson[*]
School of Chemistry, Cantocks Close, Bristol, BS8 1TS, UK

X-ray diffraction from smectic materials in device-like cells is used to determine the layer structure within the cells. The experimental method determines the smectic layer normal orientational distribution as a function of tilt and twist angles within the cell. In a special case where the layer normals are not twisted away from the alignment direction, the chevron structures have been reconstructed from the distributions. The influence of the surface pre-tilt due to the alignment layer, electric fields and skewed alignment layers on the smectic layer normal distributions are reviewed and discussed.

Keywords: surface stabilised ferrorelectric liquid crystal; X-ray diffraction; rocking curve; chevron; chiral smectic C

INTRODUCTION

To improve and develop ferroelectric liquid crystal display devices, it is important to understand the geometry of the layers within cells because it influences their optical properties. X-ray diffraction can determine directly the orientation of the layers within a cell. It has been used to demonstrate the formation of a chevron structure [1,2] in a thin cell containing smectic

The authors wish to acknowledge Robert Bannister and Ryan Heath from DERA for the manufacture of the cells, Ernie Komanschek and Gunter Grossman at Daresbury Laboratory for help with the diffraction experiments, David Rodriguez Martin at Bristol for help with some of the data analysis.

*Address correspondence to R M Richardson, H H Wills Physics Laboratory, Tyndall Avenue, Bristol, BS8 1TL, UK.

[‡]Current address: Department of Science and Engineering, University of Oxford, Parks Road, Oxford, OX1 3PJ, UK.

[†]Current address: ZBD Displays Ltd, Malvern Hills Science Park, Geraldine Road, Malvern, WR14 3SZ, UK.

C* material and the twisting of the layers within a cell (known as horizontal chevron formation). Many materials form a smectic C* on cooling from a smectic A and it is believed that the reduction in layer thickness is the primary driving force for the formation of these chevron structures. Indeed, chevron formation has been observed in the smectic A phase for materials whose layer thickness reduces on cooling through the smectic A phase [3]. Figure 1(a) shows the smectic layer spacing as a function of temperature for the commercial mixture SCE13 together with the apparent tilt angle, β, calculated from the ratio of layer spacing in the smectic C, $d_C(T)$, to the layer spacing at the lowest temperature in the smectic A, d_A.

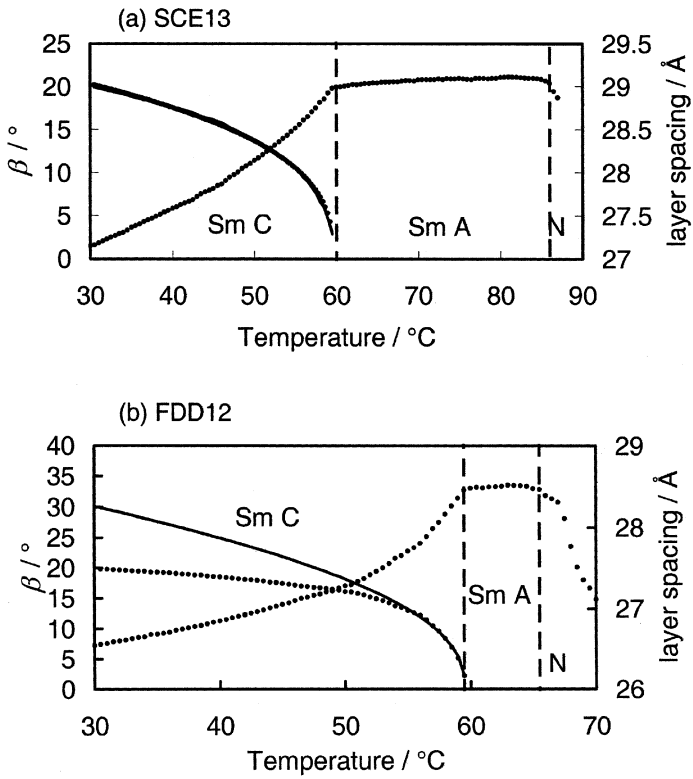

FIGURE 1 The points are the smectic layer spacing for (a) SCE13 and (b) FDD12 together with apparent molecular tilt, β, in the smectic C* phase. The lines are fits of the Landau de Gennes formula to the apparent layer tilts. For SCE13 the best-fit parameters are $\beta_0 = 47°$ and $v = 0.35$. For FDD12 they are $\beta_0 = 80°$ and $v = 0.42$ although the fit is only satisfactory near the transition.

$$\beta(T) = \cos^{-1}\frac{d_C(T)}{d_A}. \quad (1)$$

For this material, the temperature dependence of the apparent tilt angle is well described by the Landau-de Gennes formula.

$$\beta = \beta_0\left(\frac{T_{AC} - T}{T}\right)^{\nu}. \quad (2)$$

Figure 1(b) shows similar results for a proprietary mixture FDD12 which deviated much more markedly from the formula.

The standard method for observing the tilt of layers within a device using X-rays is to set the detector at twice the Bragg angle for the layer reflections and rotate the sample. The X-ray beam is only reflected into the detector when the angle of incidence onto the smectic layers is equal to the Bragg angle. Thus a plot of diffracted intensity vs. sample angle (known as a rocking curve) represents the distribution of layer normals as a function of their tilt angle. We have refined the original methodology to measure and display the full distribution of layer normals as a function of tilt and twist. This technique is outlined in section on the Experimental Method. The full effect of material and boundary conditions may be seen by inspecting the layer normal distributions. In this paper the influence of surface pre-tilt is reviewed, first. A study of the effect of an applied electric field is then presented. Finally we outline the effect of skewed alignment directions on the layer structure within a cell.

EXPERIMENTAL METHOD

The measurement consists of placing a device-like cell in a heated oven on a rotation stage in an X-ray beam. For the work reported here, the station 2.1 at the Daresbury Synchrotron Radiation Source was used. It produced a monochromatic beam (beam size: 2.0 mm × 0.8 mm) with a wavelength of 1.5 Å and the diffracted intensity was recorded on a two-dimensional position sensitive detector. An experimental run consisted of recording the diffraction from the sample in a series of frames as the sample was rotated about a vertical axis as shown on Figure 2. The incident and transmitted beam intensities were monitored by ion chambers just before and just after the sample. A typical run would take about 15 minutes.

The smectic layers only reflect the X-rays when their angle of incidence onto the layers is equal to the Bragg angle:

$$\theta_B = \sin^{-1}\left(\frac{\lambda}{2d}\right), \quad (3)$$

where λ is the wavelength and d is the smectic layer spacing. The measured

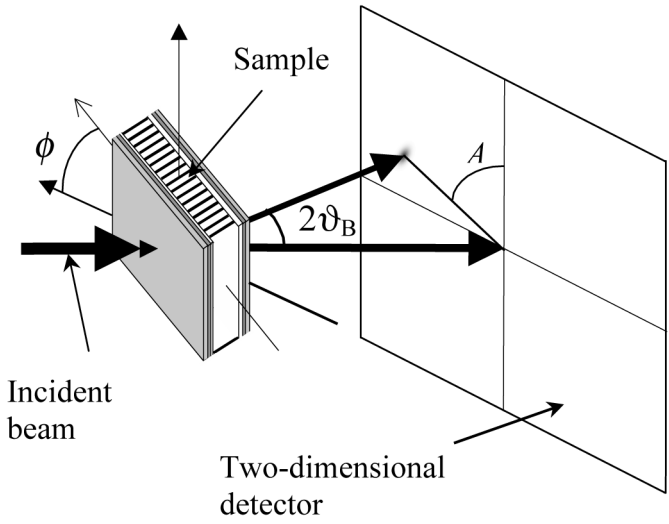

FIGURE 2 The experimental geometry for measuring the layer normal distribution of a device like cell. The rubbing direction of the alignment layers is horizontal.

Bragg intensity, $I(\phi, A)$ may therefore be transformed into the distribution of layer normals as a function of the twist and tilt angles, $n(\gamma, \delta)$. The following equations are the relationships between the physically measured angles, ϕ, θ_B and A, and the direction of the layer normal. They may be derived easily by considering the geometry of the diffraction process and are essentially corrections for the curvature of the Ewald sphere.

$$\sin\delta = \sin\theta_B \cos\phi - \cos\theta_B \sin\phi \sin A, \tag{4}$$

$$\tan\gamma = \frac{\tan\theta \sin\phi}{\cos A} + \cos\phi \tan A. \tag{5}$$

The data reduction takes place in four stages, which have been described in detail elsewhere [4]. Firstly, the frame corresponding to $\phi = 0$ is determined from the measured transmission of the sample as a function of the frame number. The frames were taken at sample angles incremented by a fixed amount ($\Delta\phi$) so the transmission varies with frame number, j, as follows:

$$T_j = S \exp\left(-\frac{a}{\cos(\Delta\phi(j - j_0))}\right), \tag{6}$$

where a is the absorbance of the sample for a beam perpendicular to it, S is a scale factor to account for different ion chamber efficiencies and j_0 is the frame number for which the X-ray beam would be perpendicular to

the surface. The expression (6) was fitted to the measured transmissions with S, a and j_0 as variable parameters in order to determine j_0. The sample angle for frame number, j, was then determined by the equation:

$$\phi = (j - j_0)\Delta\phi. \tag{7}$$

The second stage is to divide the counts in each frame by T_j to correct for the variation in self-shielding due to the different path lengths of the beam through the sample.

The third stage is to determine the Bragg intensity vs sample angle, ϕ, and azimuthal angle, A. In each frame, the corrected counts in pixels with scattering angles in an interval near twice the Bragg angle were grouped. They were grouped into bins of equal increment of azimuthal angle as indicated in Figure 3. Since some of the square pixels of the detector were only partly inside the new bins, a procedure to subdivide the pixels on the bin border was devised. At this stage a background was determined from regions of the same azimuthal angle but slightly lower and higher scattering angles. It was subtracted from the counts in the group before they were summed to give, I(ϕ, A).

Finally, for each point on the distribution, the values of the layer tilt angle, δ, and the twist angle, γ, were then calculated from the values of ϕ and A using Eqs (4) and (5). The final layer normal distribution was plotted as a false color contour such as that shown in Figure 4.

We believe this is the most effective way to display the layer structure of a cell because it shows the complete two-dimensional layer normal distribution in one diagram. In the special cases where there is no twist of the layers, the only peak in the contour diagram will be at $\gamma = 90°$ (or 270° for

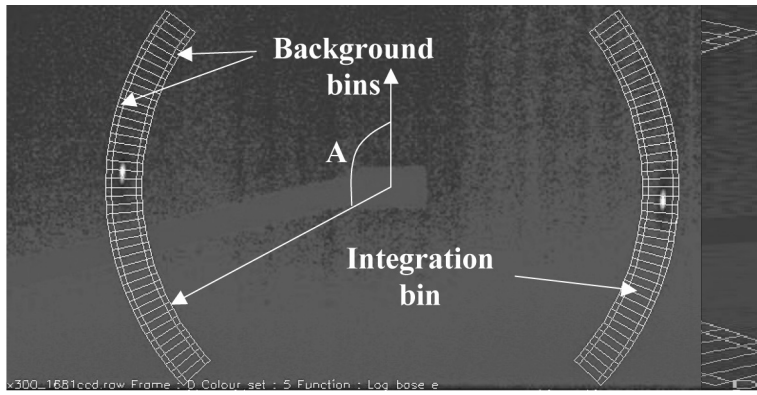

FIGURE 3 Typical diffraction pattern from smectic liquid crystal showing the bins used to regroup into $I(\phi, A)$.

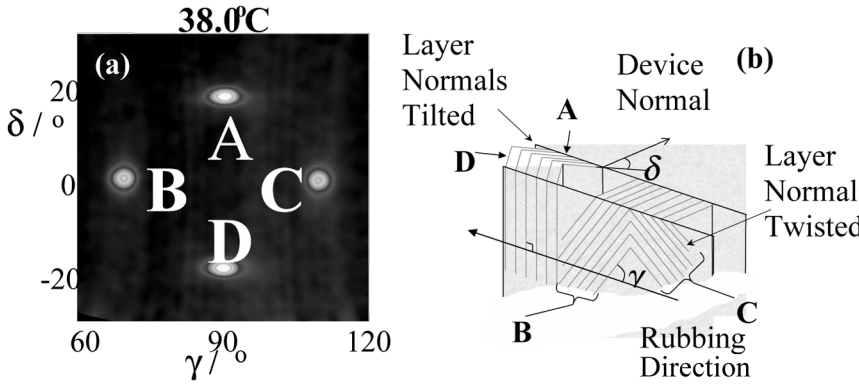

FIGURE 4 (a) A layer normal distribution measured from a region of a cell with many needle defects. There are four peaks. A and C correspond to a chevron structure with tilted layers. B and D correspond to twisted or rotated layers. In (b) these layer orientations are illustrated.

the opposite member of the Friedel pair of reflections). The intensity at each value of δ may then be integrated over γ to obtain a one-dimensional layer normal distribution vs. δ. If the layers are not twisted within the cell, the one-dimensional layer normal distribution may also be obtained more directly by integration of the Bragg intensity in each frame. The correction for the Ewald sphere curvature is also much simpler since $A = 90°$ or 270° so $\delta = \phi - \theta_B$.

A one-dimensional layer normal distribution may be interpreted qualitatively as shown in Figure 5. For instance, a single peak at $\delta = 0$ indicates only one layer orientation perpendicular to the cell walls, that is bookshelf geometry. Two peaks at $\delta = \pm\psi$ indicate a symmetric chevron structure with the the arms tilted by $\pm\psi$. A constant level indicates a continuum of orientations, corresponding to curved layers. Figure 6 shows a typical result.

In the special case where the layers are only tilted, and not twisted, it is possible to reconstruct the shape of the layer structure if a few assumptions are made. First we assume that the tilt angle changes monotonically across the thickness of the cell and that the layer normal distribution corresponds to a single domain. Secondly we assume that there is no intrinsic angular broadening of the Bragg reflection from the smectic layers. Since the height of the layer normal distribution is measured at a number, N, of discrete points it is possible to reconstruct the layer structure as a series of steps, $(\Delta x_i\, \Delta y_i)$, which describe the locus of a layer in the cell. For every small displacement across the thickness of the cell, Δx_i, a layer has a corresponding displacement, Δy_i, along the rubbing direction of the cell.

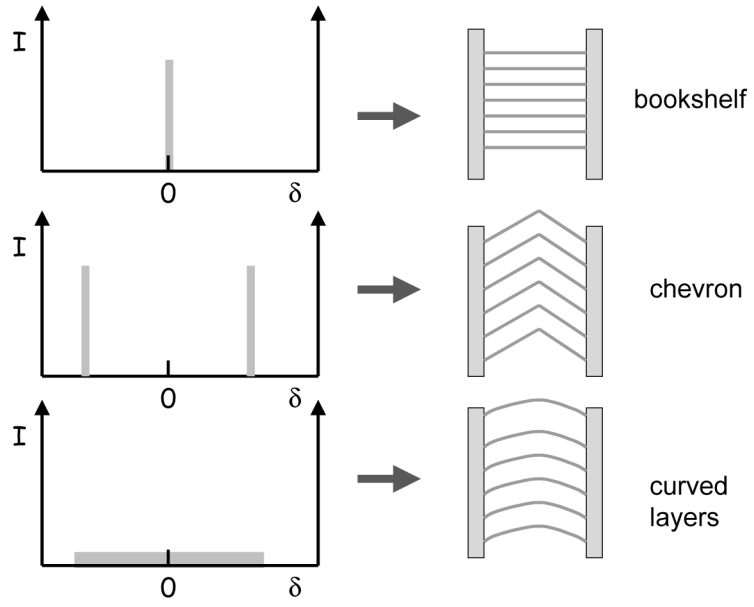

FIGURE 5 Interpretation of 1-dimensional layer normal distribution in terms of layer structure in cell.

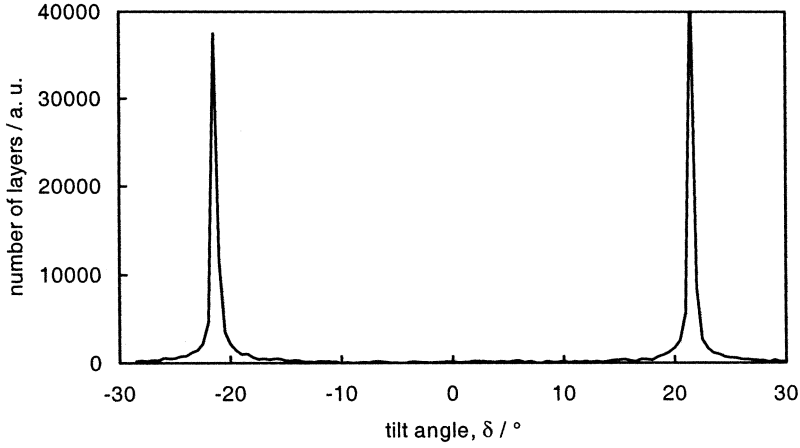

FIGURE 6 1-dimensional layer normal distribution of SCE13 at room temperature in a parallel aligned cell.

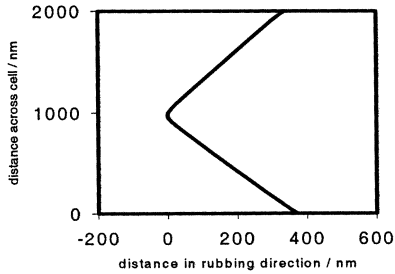

FIGURE 7 Layer structure reconstructed from layer normal distribution in Figure 6.

The height of the layer normal distribution, $n(\delta_i)$, is proportional to the volume of smectic material inclined at an angle of δ_i, so the two displacements will be given by the formulae,

$$\begin{aligned} \Delta x_i &= bn(\delta_i) \sin \delta_i, \\ \Delta y_i &= bn(\delta_i) \cos \delta_i, \end{aligned} \tag{8}$$

where b is a constant defined by the condition that the total number of Δx_i steps must sum to the cell thickness (usually 2 μm). Figure 7 shows a layer structure reconstructed from the layer normal distribution shown in Figure 6. We believe this is a useful process for visualizing the form of the layers within a cell. However its limitations should also be considered. For instance, if the slope is not assumed monotonic, other structures would be equally consistent with the measured layer normal distribution. Also, if the X-ray beam were illuminating different domains in the cell, equal areas of oppositely tilting layers would be indistinguishable from the chevron structure using this X-ray technique. However, optical inspection of the cell may be able to eliminate this possibility. The assumption of no intrinsic broadening is unlikely to be exactly true. The Bragg reflection from smectic layers does have an intrinsic width that results from the one-dimensional nature of the smectic ordering. This means that any curves or angles in the reconstructed structure may be slightly more rounded than in the real structure.

SURFACE PRE-TILT EFFECTS IN ANTI-PARALLEL CELLS

For cells in which the alignment directions of the two cell walls are anti-parallel, there is the possibility of forming uniformly tilted layers as well as chevron structures. In the smectic A phase, experiments with different alignment layers have shown that a uniformly tilted layer is generally formed and there is a good correlation between its tilt angle, δ_A, and

the pre-tilt of the director measured in the nematic phase. The SE130 alignment layers gave $\delta_A \sim 1°$, SE610L gave $\delta_A \sim 8°$ and evaporated silicon monoxide gave $\delta_A \sim 21°$ which were all within a few degrees of the pre-tilt measured optically using E7 nematic mixture [5]. On cooling into the smectic C phase, the reduction in layer thickness drives changes in the orientation of the layers. It has been established that there is a strong tendency for the if the layer pitch (i.e. the number of layers per unit length of the cell) to remains constant [6]. This can be achieved if the tilt angle in the smectic C phase has the value given by the formula:

$$\delta_C = \pm \cos^{-1}\left(\cos \delta_A \frac{d_C(T)}{d_A}\right). \tag{9}$$

However, the sign of δ_C might be the same or opposite to that of δ_A and the possibility of the layers twisting must also be considered. If the sign of δ_C is the same as δ_A, a uniformly tilted layer structure is expected and if it is opposite, a chevron structure may result. Figure 8 shows a comparison of the layer normal distributions from well aligned regions of cells made with three different alignment layers. The low and medium pre-tilt alignment layers gave two peaks in the layer normal distribution whereas the high pre-tilt alignment layer gave only one peak suggesting a uniformly tilted layer structure.

It is possible to rationalize this behavior with the following model. The angle between the molecular director and the layer normal (i.e. the cone angle, Θ) is generally rather larger than the apparent tilt angle, β, deduced from the layer spacing.

$$\Theta = (1 + x)\beta, \tag{10}$$

where for SCE13 x has been found to be about 0.1. Since we know $\beta(T)$ from measurements of the layer spacing, it is possible to calculate the cone angle as

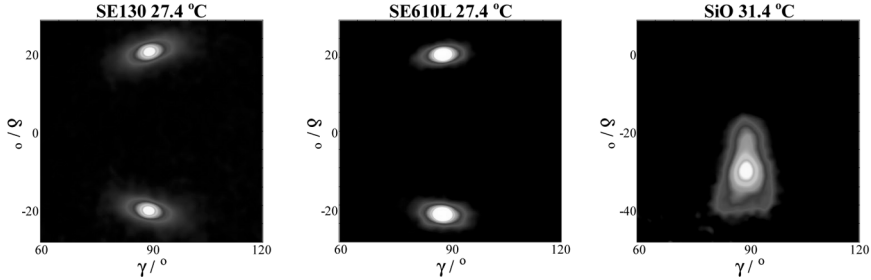

FIGURE 8 Layer normal distributions from SCE13 at room temperature in anti-parallel aligned cells. The alignment layers impose low (SE130), medium (SE610L) and high (SiO) pre-tilts on the director.

a function of temperature. The possible orientations of the molecular director for which the director is not twisted away from the rubbing direction are

$$\Omega = \delta_C \pm \Theta \text{ or } \Omega = -\delta_C \pm \Theta, \tag{11}$$

where δ_C is taken as positive so there are four possible values for the discrepancy between the molecular director of the bulk, Ω, and that defined by the surface which is measured as the layer tilt in the smectic A phase, δ_A. As an example, the values for SCE13 in a high pre-tilt (silicon monoxide aligned) are plotted in Figure 9.

The branches starting from zero discrepancy in the smectic A correspond to a layer uniformly tilted in the same sense as in the smectic A. The other two branches correspond to a layer tilted in the opposite sense which would be consistent with chevron formation. In this example, the lowest discrepancy at all temperatures is for the uniformly tilted layer as is observed to form at room temperature for a high pre-tilt cell. The same model can also explain qualitatively the appearance of a chevron at 40°C in medium pre-tilt cells [5].

THE EFFECT OF APPLIED ELECTRIC FIELD

Background

There has been a large amount of work on the effect of applied fields above the usual switching region ($>1\,\mathrm{V\mu m^{-1}}$). Hartmann [7] *et al.* suggested that the reorientation of layers at a chevron interface was easy compared to

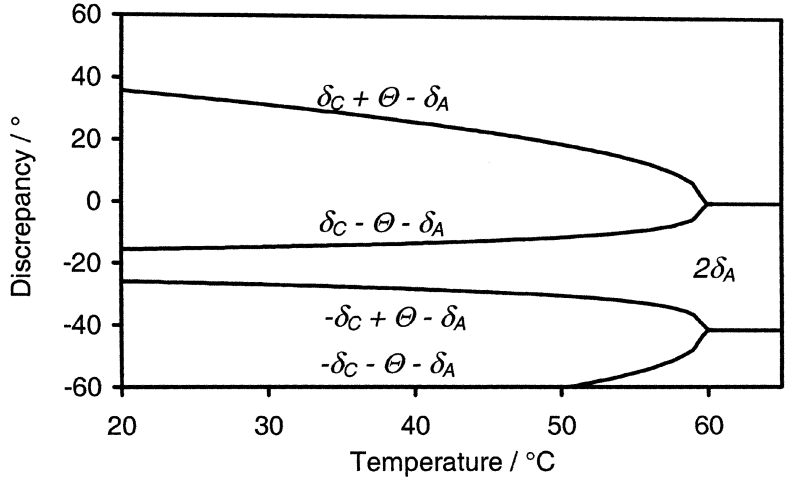

FIGURE 9 Four possible discrepancies between the surface and bulk orientation of SCE13 in a high pre-tilt cell.

those at the alignment layer boundaries and so application of a field would deform the chevron. Sato *et al.* [8] showed that application of a large AC electric field to a device induced a striped optical texture which X-rays showed to be pseudo-bookshelf. This is now called the electric field induced stripe texture (EFIST) to distinguish it from the needle texture which is often found in low-tilt cells. Similar effects were observed by Johno *et al.* [9] who called it smectic layer switching.

Srajer, Pindak and Patel *et al.* [10] also used X-ray diffraction to elucidate the structure of the smectic layers in a SSFLC device after electric field treatment. Unfortunately they did not present any optical texture with the X-ray results and so it cannot be assumed to be representative of the EFIST. The technique that they used did not only give the layer tilt, δ, of the smectic layers at $\gamma = 90^\circ$ but also the layer twist, γ, at $\delta = 0^\circ$. This new information showed that the pseudo bookshelf, seen in their sample, consisted of two domains where the layers were rotated by $\pm$ cone angle in the SmC* phase. For such a reorientation to take place Srajer argued that there must be some degree of molecular flow. This type of layer reorientation has been extensively studied by Dierking *et al.* [11–16]. Smectic layers, originally in the classical chevron geometry, that have forced into the bookshelf configuration and reoriented to an angle where $\gamma \neq 90^\circ$ by the application of an oscillating electric field are often referred to as rotated layers. There are two different types of rotated layer, limited and continuous. Limited rotated layers rotate to a maximum angle of $\gamma = 90^\circ \pm$ cone angle, indicating that the director remains in the alignment direction. It is therefore unsurprising that this type of layer reorientation usually occurs in devices with high surface anchoring energies. Limited rotated layers have also been referred to as horizontal chevrons because of their optical texture. Continuous rotated layers are not constrained and continue to rotate up to large angles given sufficient duration of the applied field. Many factors for the rate and type of rotation have been studied but as yet there has not been a mechanism suggested, although it is clearly linked to molecular switching.

Vorflusev *et al.* [17] explained the origins of the forces that shaped the smectic layer structure in the EFIST. His optical measurements led him to conclude that there was a curvature deformation along the smectic layer perpendicular to the alignment direction. He believed that the EFIST was a kind of electrohydrodynamical instability similar to those existing in nematics with oblique boundary tilt of the director.

Many other studies of EFIST have been performed. For instance, Itoh *et al.* [18] showed there was a sudden change in the rate of change of dielectric permittivity when the EFIST was observed, implying a large change in smectic layer structure. Bryant *et al.* [19] used time resolved X-ray diffraction to follow the evolution of layer deformation and Hikmet

et al. [20] used a novel X-ray technique to follow the deformation of the layers as an oscillating electric field was applied. Finally, Beresnev *et al.* [21] observed a different electric field induced stripe texture where the stripes formed perpendicular to the alignment direction. In the next sections we report X-ray diffraction experiments to determine two-dimensional layer normal distributions for the structures inside a device subjected to high electric field treatment.

The effect of electric field on a surface stabilized ferroelectric liquid crystal has been made using a material with various concentrations of a chiral dopant. The aims were to show the dependence of layer deformation on the magnitude of spontaneous polarization and to determine the effect of increasing field on the layer structure. The results are consistent with those in the papers cited and expand upon them.

Experimental Results

The cells used for this study had rubbed polymer alignment layers, aligned parallel, and indium tin oxide electrodes for the application of the electric field (100 Hz square wave). The host material was a proprietary mixture, FDD12, combined with three different proportions of the same chiral dopant (1.5%, 3.0% and 6.0% by weight). The phase sequence of FDD12 is as follows:

$$\mathrm{SmC}^* \leftrightarrow 58^\circ\mathrm{C} \leftrightarrow \mathrm{SmA} \leftrightarrow 66^\circ\mathrm{C} \leftrightarrow \mathrm{N}^* \leftrightarrow 69^\circ\mathrm{C} \leftrightarrow \mathrm{I}.$$

The spontaneous polarization at 3.0% doped was approximately $14\,\mathrm{nCcm}^{-2}$.

Figure 10 shows some layer normal distributions from a series of measurements on FDD12 (3% doped) in which the applied voltage was increased in steps but with zero volts measurements interleaved. The measurements were made at ambient temperature, 27°C and no change in the smectic layer spacings were observed throughout. Figure 10(a) shows peaks at $\delta = -23.2^\circ$ and $\delta = 21.7^\circ$ and $\gamma = 90^\circ$ indicating that the initial state of the cell was a chevron (with arms at -23.2° and 21.7°) with no rotation of the layers. As the applied voltage was increased to $13.75\,\mathrm{V\mu m}^{-1}$, the peaks in the layer normal distribution develop shoulders at lower values of δ as shown in Figures 10(b) and (c). These shoulders correspond to layers tilted by smaller amounts than the original chevron but since the layer normal distribution remains at zero at $\delta = 0^\circ$ there are no layers in the bookshelf configuration. These shoulders indicate that the layers are curving but that the chevron apex is retained. Figure 10(d) shows that at an applied field of $15\,\mathrm{V\mu m}^{-1}$ there are layers with $\delta = 0^\circ$ indicating that the chevron apex has been lost but a substantial number of layers remain at

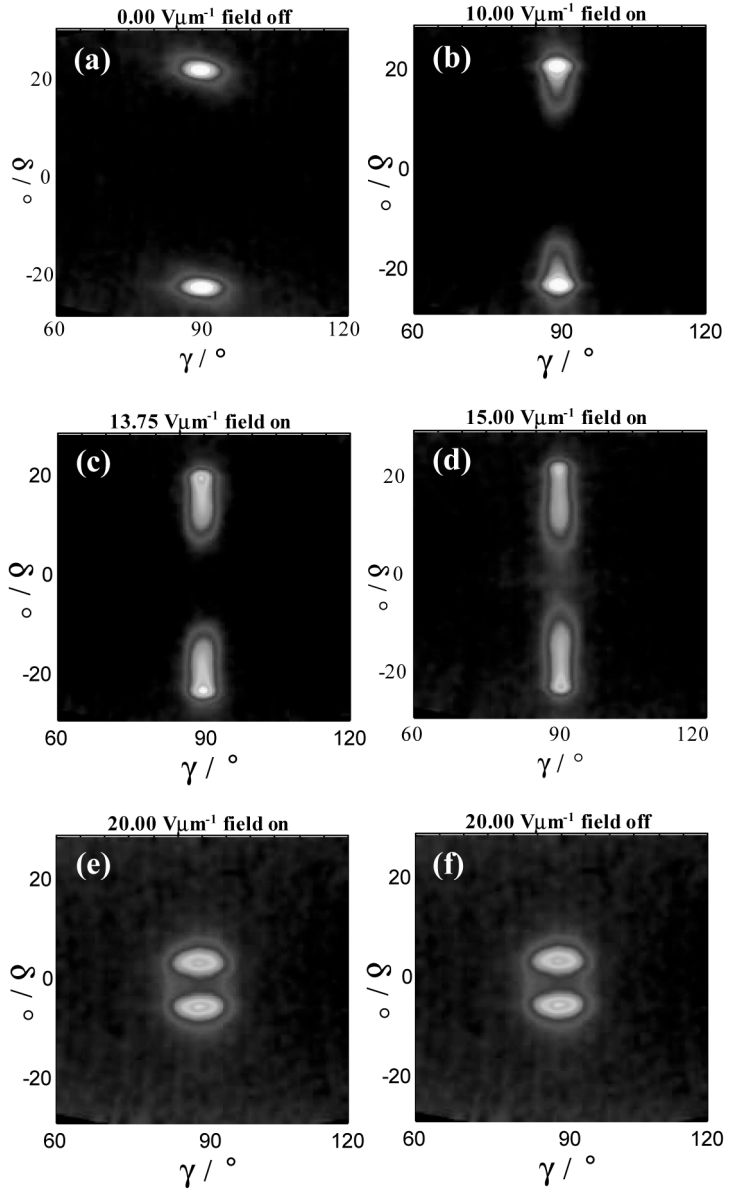

FIGURE 10 Layer normal distributions for FDD12 with applied fields of (a) $0\,V\mu m^{-1}$ (b) $10.0\,V\mu m^{-1}$ (c) $13.75\,V\mu m^{-1}$ (d) $15.0\,V\mu m^{-1}$ (e) $20\,V\mu m^{-1}$ and (f) with the field removed after applying $20\,V\mu m^{-1}$.

the original chevron angles. These results are consistent with a bending of the layers near the chevron apex with the layers near the surface remaining at the same orientation. The progressive changes in the shape of the chevrons as the field increases have been visualized in the reconstructed layer structures shown in Figure 11. It can be seen that the chevron apex is lost by about $15\,\mathrm{V\mu m^{-1}}$ but the layer orientation remains fixed near the surface for fields up to $17.5\,\mathrm{V\mu m^{-1}}$. These deformations are not reversible in that the zero volts layer normal distributions were very similar to those with the field applied.

Thus, although a coupling between the spontaneous polarization and the electric field is driving the formation of a pseudo-bookshelf structure, the structure is stabilized by another force(s).

On further increasing the field to $18.25\,\mathrm{V\mu m^{-1}}$ and $20.0\,\mathrm{V\mu m^{-1}}$, there is sudden change in the layer normal distribution which is also non-reversible as shown in Figures 10(e) and (f). At this point, the sample shows the EFIST as shown in Figure 12. The peaks in the layer normal distribution are now at $\delta \sim \pm 4^\circ$ but broadened, especially in the γ direction. The orientation of the layers near the surface has drastically changed implying that the surface alignment is now lost. The broadness of the peaks in γ is consistent with undulations of the layers in a direction perpendicular to the field as suggested by Vorflusev as a result of an electrohydrodynamic instability. This is illustrated in Figure 13. It is not clear why the tilt of $\pm 4^\circ$ is preferred. Since the coupling between the spontaneous polarisation and

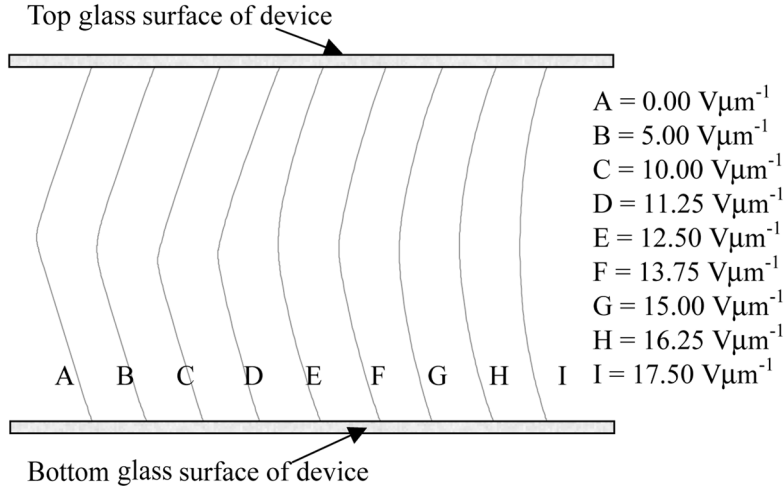

FIGURE 11 Reconstructed layer structures for FDD12 in a cell with a field applied.

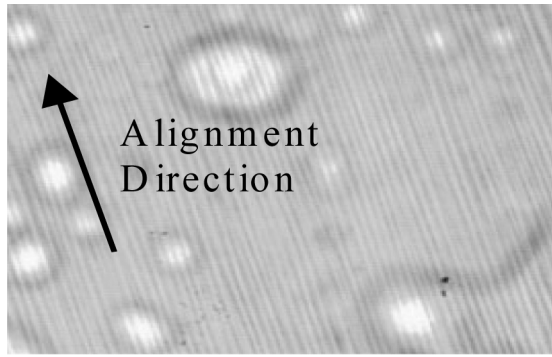

FIGURE 12 Electric field induced stripe texture (EFIST) in same cell as for results in Figure 10.

the field tends to zero as the layer tilt angle tends to zero, the force will drive the structure to bookshelf will be relatively weak for such a low tilt. It is possible that the tilt of 4° is simply the point where the resistance to reorientation balances the electric force.

The cells with other doping levels confirm this picture. For 6% doping, the layer bending takes place at slightly lower fields than the 3% as shown

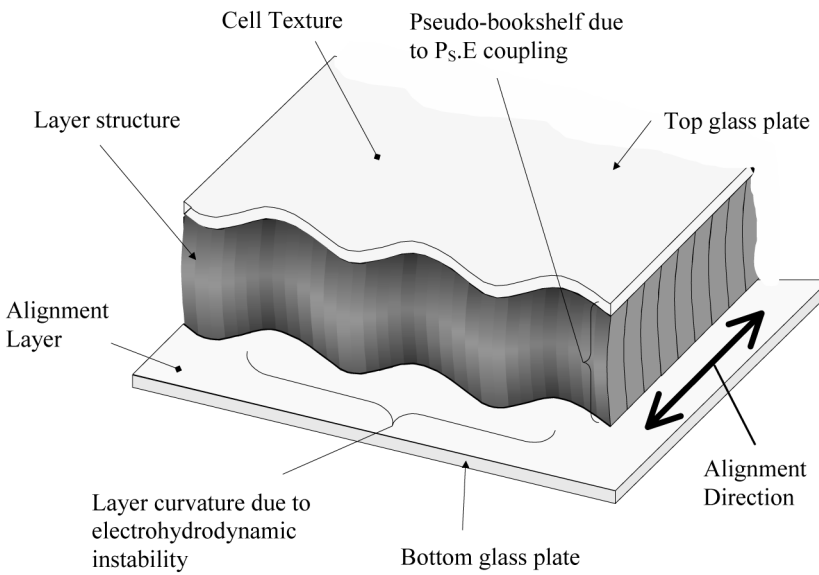

FIGURE 13 Illustration of the optical texture and layer structure of the cell during the application of $20\,V\mu m^{-1}$.

the 10.0 $V\mu m^{-1}$ result in Figure 14(a) which is comparable with 13.75 - $V\mu m^{-1}$ for 3% (Fig. 10(c)). However, the 6% doped material does not go through the pseudo bookshelf stage. By 25.0 $V\mu m^{-1}$ there is a single peak in the distribution, spread out in γ, corresponding to an undulating bookshelf structure similar to that shown in Figure 13. Close inspection of this peak reveals a small preference for the layers to be rotated away from the rubbing direction by $\sim 5^{\circ}$. Further increase of the field has little effect until about 60 $V\mu m^{-1}$ (Fig. 14(c) and (d)) when there is an abrupt increase in γ indicating further rotation of the layers. For 1.5% doping, the torque from the coupling of the field to the spontaneous polarisation is expected to be less. If fact, layer normal distribution corresponding to a simple chevron structure was found for fields up to 25.0 $V\mu m^{-1}$ (Fig. 15(a)). At higher

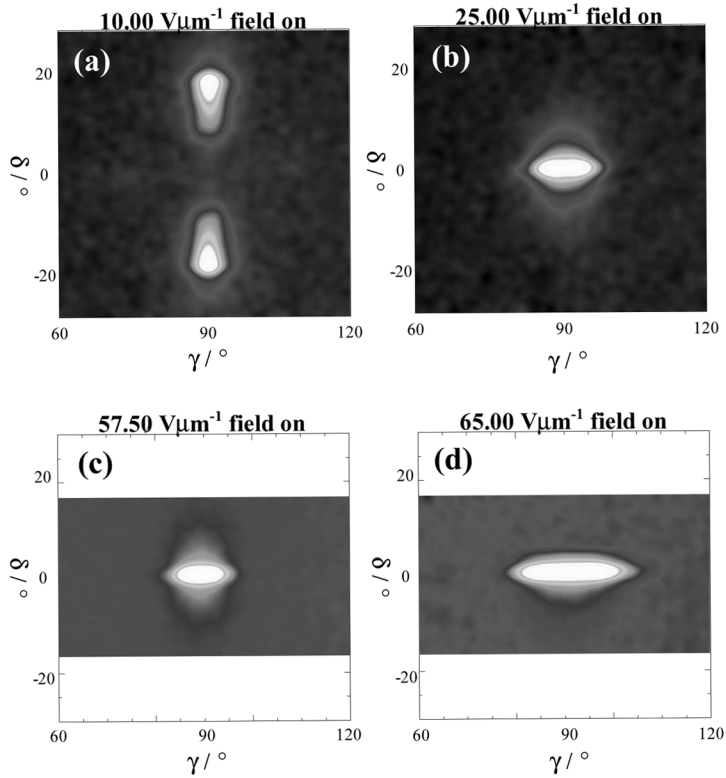

FIGURE 14 Layer normal distribution from FDD12 with 6% of chiral dopant. (a) shows a distorted chevron 10 $V\mu m^{-1}$; (b) and (c) shows bookshelf with limited rotation from 25 $V\mu m^{-1}$ to 58 $V\mu m^{-1}$ and (d) shows more layer rotation at 65 $V\mu m^{-1}$ and above.

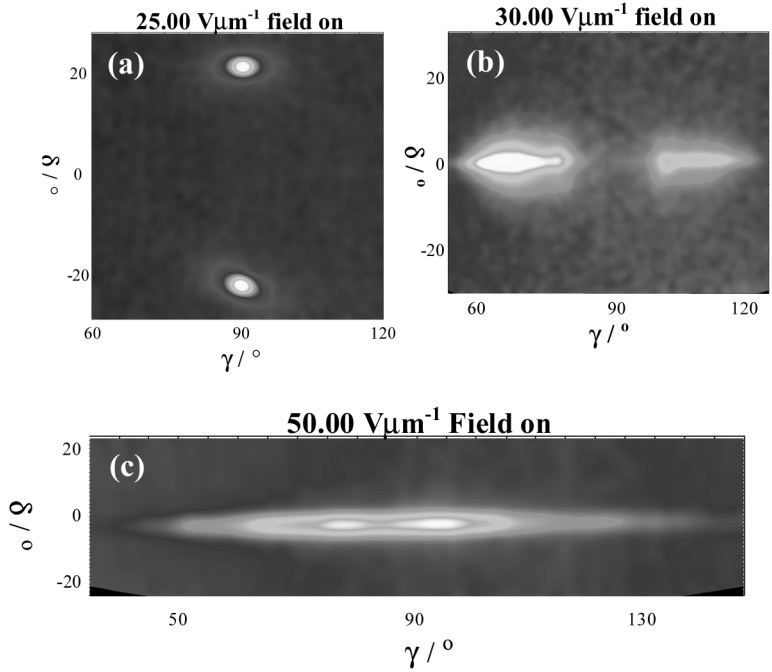

FIGURE 15 Layer normal distributions from FDD12 with 1.5% of chiral dopant. (a) shows a chevron is retained with 25 $V\mu m^{-1}$; (b) shows limited rotated bookshelf structure and (c) show unlimited rotated bookshelf structure.

fields (eg Fig. 15(b): 30.0 $V\mu m^{-1}$), there is no EFIST observed optically but a sudden transition to a bookshelf with rotated layers. The layers are rotated by approximately the cone angle ($\sim 20°$) suggesting that the molecules are oriented parallel to the original rubbing direction. At still higher fields (eg Fig. 15(c): 50.0 $V\mu m^{-1}$) the distribution becomes very broad suggesting that the kinetic energy from the switching process is now sufficient to rotate the molecules away from the rubbing direction.

Conclusions Regarding Electric Field Effects

The results outlined above have shown that the layers near the alignment layer surface are more strongly anchored than those at the chevron interface because they require a higher field to reorientate, supporting the ideas originally put forward by Hartmann *et al.* They also show that the electric field induced stripe texture is an undulation of the layers (as described by Vorflusev *et al.*) that forms when the influence of the

alignment layer is overcome by the applied field. The periodicity of the layers at the surface is changed from that of the smectic A phase to a value very slightly above that of the smectic C* phase.

The study of FDD12 containing three different concentrations of chiral dopant indicated that there was a relationship between spontaneous polarisation, rotated layers and the EFIST layer structure. If the P_s is sufficiently small the P_s. E coupling force is unable to overcome the layer elasticity or the surface anchoring and neither layer curvature nor the EFIST is developed. Then the only mechanism capable of deforming the layer is the molecular flow caused by the high field switching we have described. This can enable limited layer rotation (i.e. up to the cone angle from the rubbing direction) if the surface anchoring is strong and continuous layer rotation if the surface anchoring is overcome.

SKEWED CELL CONSTRUCTION

Chevron formation has been one of the major limitations to the development of display devices based on smectic C* liquid crystals. The chevron structure compromises the optical properties of a cell because the director is not necessarily in the plane of the cell and because of the possibility of optical defects associated with boundaries between oppositely pointing chevrons. One way to form a bookshelf structure was introduced by Patel [22]. He applied an AC field during cooling from the smectic A phase to disrupt the surface alignment and was able to prepare cells with layers at the cone angle to the alignment direction and in bookshelf geometry. However, there were drawbacks to this method in that high switching voltages were required and bistability was reduced. He therefore suggested fabrication of a cell with the top and bottom plates rotated by twice the cone angle with respect to each other. For this reason we have explored the geometry of skewed cells.

For these measurements, the commercial mixture, SCE8 was used in cells that were aligned with low pre-tilt SE130 alignment layers. The rubbing directions were aligned parallel and with skew angles of 10°, 20°, 45° and 67° between them. Measurements were made at a series of temperatures from the smectic A phase to room temperature (30°C).

The layer normal distributions from the parallel cell were consistent with the standard picture. That is a bookshelf structure with layers perpendicular to the rubbing direction in the smectic A and a chevron in the smectic C phase. In the skewed cells, a bookshelf twisted by half the skew angle was generally found in the smectic A and a similarly twisted chevron in the smectic C. Figure 16 shows the layer normal distributions for the cell skewed by 20°, indicating a bookshelf structure twisted by 10° and a

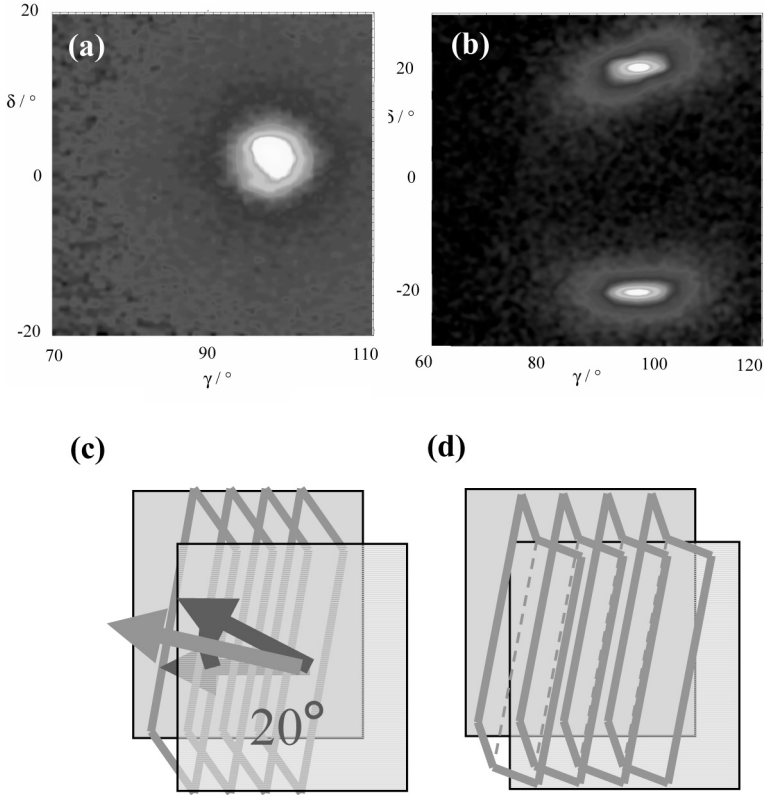

FIGURE 16 Layer normal distributions from SCE8 in a cell with the alignment directons skewed by 20°. (a) at 70°C in the SmA phase and (b) at 30°C in the SmC phase. (c) and (d) illustrate the corresponding twisted bookshelf and chevron structures.

chevron twisted by a similar amount. The only exception to this behavior is the 45° skewed cell which indicates that the layers are curved in the smectic A phase and that the two parts of the chevron in the smectic C are twisted by different angles (25° and 32°). Figure 17 shows the corresponding layer normal distributions.

These observations can be rationalized by assuming that a smectic A domain grows from a twisted nematic on cooling. It is nucleated in the centre of the cell at an intermediate angle. The smectic C simply forms a chevron at the pre-determined twist angle. The 45° result is probably representative of more than one domain which have nucleated at different angles.

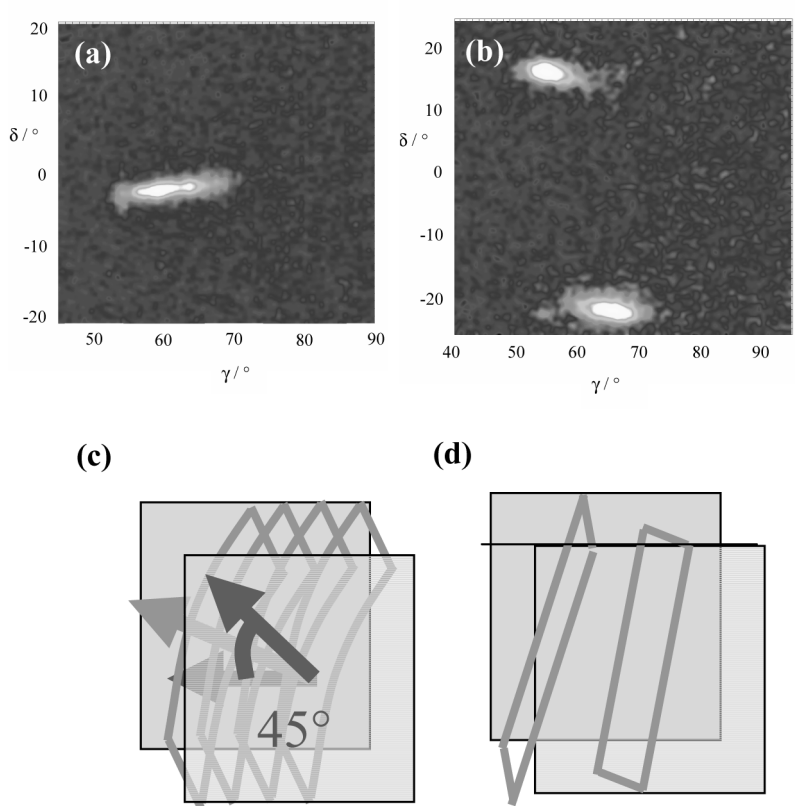

FIGURE 17 Layer normal distributions from SCE8 in a cell with the alignment directons skewed by 45°. (a) at 70°C in the SmA phase and (b) at 30°C in the SmC phase. (c) and (d) illustrate the corresponding twisted bookshelf and chevron structures.

CONCLUSIONS

X-ray diffraction is the only way to determine the distribution of layer orientations in a device-like cell. We have found it useful to present the distribution of layer normals as a two dimensional contour map of number of layers vs. the tilt and twist (or rotation) angles. In this paper, we have reviewed results which demostrate the effect of surface pre-tilt due to the alignment layers and explain whether a chevron or uniform layer structure is formed. The results from field alignment show a complex process in which the layers are first bent to a pseudo-bookshelf geometry and are then unpinned from the surface at higher fields. At still higher fields layer

rotation is also observed. The influence of the strength of the spontaneous polarisation on these processes has been demonstrated. Finally skewed cell construction has been explored. Here, the layer structure is consistent with the smectic phase growing from the centre of the cell with the surface forces only being responsible for the initial twisted nematic. Future experiments to determine the influence of electric field on the surface layers in such cells are planned.

REFERENCES

[1] Rieker, T. P., Clark, N. A., Smith, G. S., Parmar, G. S., Sirota, E. B., & Safinya, C. R. (1987). *Phys. Rev. Lett.*, *59*, 2658.
[2] Ouchi, Y., Lee, J., Takezoe, H., Fukuda, A., Kondo, K., Kitamura, T., & Mukoh, A. (1988). *Jap. J. Appl. Phys.*, *27*, L725.
[3] Taylor, L., Richardson, R. M., Ebbutt, J., & Jones, J. C. (1995). *Mol. Cryst. Liq. Cryst.*, *263*, 255–270.
[4] Jenkins, S. A. (2000). Thesis, University of Bristol.
[5] Jenkins, S. A., Jones, J. C., Dunn, P. E., & Richardson, R. M. (2000). *Ferroelectrics*, *244*, 83–93.
[6] Rieker, T. P., Clark, N. A., Smith, G. S., & Safinya, C. R. (1989). *Liq. Cryst.*, *6*, 565.
[7] Hartmann, W. J. A. M. & Luyckx-Smolders, A. M. M. (1990). *J. Appl. Phys.*, *67*, 1253.
[8] Sato, Y., Tanake, T., Kobayashi, H., Aoki, K., Watanabe, H., Ouchi, Y., Takazoe, H., & Furukawa, K. (1989). *Jap. J. Appl. Phys.*, *28*, L483.
[9] Johno, M., Chandani, A. D. L., Ouchi, Y., Takezoe, H., Fukuda, A., Ichihashi, M., & Furukawa, K. (1989). *Jap. J. Appl. Phys.*, *28*, L119.
[10] Srajer, G. S., Pindak, R., & Patel, J. S. (1991). *Phys. Rev. A*, *43*, 5744.
[11] Dierking, I., Komitov, L., & Lagerwall, S. T. (1998). *Jpn. J. App. Phys. Pt. 2*, *37*, L57.
[12] Dierking, I., Komitov, L., & Lagerwall, S. T. (1998). *Jpn. J. App. Phys. Pt. 2*, *37*, L525.
[13] Dierking, I., Gießelmann, F., & Zugenmaier, P. (1997). *Ferroelectrics*, *198*, 41.
[14] Dierking, I., Komitov, L., & Lagerwall, S. T. (1998). *Liq. Cryst.*, *24*, 775.
[15] Dierking, I., Komitov, L., & Lagerwall, S. T. (1998). *Liq. Cryst.*, *24*, 769.
[16] Dierking, I., Gießelmann, F., Schacht, J., & Zugenmaier, P. (1995). *Liq. Cryst.*, *19*, 179.
[17] Vorflusev, V. P., Panarin, YU. P., Pikin, S. A., & Chigrinov, V. G. (1993). *Liq. Cryst.*, *14*, 1055.
[18] Itoh, N., Koden, M., Miyoshi, S., Wada, T., & Akahane, T. (1994). *Jap. J. Appl. Phys. Part 2 (Letters)*, *33*, 241.
[19] Bryant, G. K. & Gleeson, H. F. (1998). *Ferroelectrics*, *214*, 709.
[20] Hikmet, R. A. M. (1995). *Liq. Cryst.*, *18*, 927.
[21] Beresnev, L. A., Schumacher, E., Pikin, S. A., Fan, Z., Ostrovsky, B. I., Hiller, S., Onokhov, A. P., & Haase, W. (1995). *Jpn. J. Appl. Phys.*, *34*, 2404.
[22] Patel, J. S., Lee, S-D., & Goodby, J. W. (1989). *Phys. Rev. A*, *40*, 2854.